APL Materials

# Preparation and uses of large area single crystal metal foils

Cite as: APL Mater. **7**, 100905 (2019); https://doi.org/10.1063/1.5114861
Submitted: 12 June 2019 • Accepted: 03 October 2019 • Published Online: 25 October 2019

Sunghwan Jin and Rodney S. Ruoff

# Preparation and uses of large area single crystal metal foils

Cite as: APL Mater. 7, 100905 (2019); doi: 10.1063/1.5114861
Submitted: 12 June 2019 • Accepted: 3 October 2019 •
Published Online: 25 October 2019



Sunghwan Jin[1,a] and Rodney S. Ruoff[1,2,3,4,a]

## AFFILIATIONS

[1]Center for Multidimensional Carbon Materials (CMCM), Institute for Basic Science (IBS), Ulsan 44919, South Korea
[2]Department of Chemistry, Ulsan National Institute of Science and Technology (UNIST), Ulsan 44919, South Korea
[3]School of Materials Science and Engineering, Ulsan National Institute of Science and Technology (UNIST), Ulsan 44919, South Korea
[4]School of Energy and Chemical Engineering, Ulsan National Institute of Science and Technology (UNIST), Ulsan 44919, South Korea

[a]**Authors to whom correspondence should be addressed:** sunghwanjin00@gmail.com; jinsh1@ibs.re.kr; ruofflab@gmail.com; and rsruoff@ibs.re.kr

## ABSTRACT

Various preparations and uses of single crystal metals are discussed. We briefly review (i) preparation methods of single crystal metals such as growth from melts, epitaxial deposition in vapors and solutions, and abnormal grain growth in solids and (ii) uses of single crystal metals according to their produced shapes ("bulk" vs "film and foil"). We pay special attention to recent advances in the preparation of large area single crystal metal foils and their potential uses.



## INTRODUCTION

A grain in metallurgy is a small or microscopic single crystal, which has a periodic arrangement of atoms. Most metals in general use are polycrystalline, thus consisting of grains separated by grain boundaries (GBs), whereas single crystal metals have a single grain throughout the entire sample and have no GBs. Single crystal metals have different properties and uses than their polycrystalline counterparts. For example, they have anisotropic properties (e.g., elastic constants, linear thermal expansion, linear compressibility, and electrical resistance), while randomly oriented polycrystalline metals usually have isotropic properties.[1] The mechanics of single crystal metals differ from polycrystalline metals because the strength of a metal is strongly related to the size of the grain. During deformation, dislocations propagate in the grain through the appropriate slip systems and GBs impede their motion so that they "pile up" at GBs. This limits the plasticity and hence increases the yield strength of metals. Single crystal metals with extremely large grains are generally weaker and more ductile than polycrystalline metals.[2] GBs in polycrystalline metals scatter electrons so that single crystal metals have a higher electrical conductivity at room temperature. The scattering of electrons at GBs is temperature dependent because it is related to electron-phonon coupling, but it has been found that at temperatures below about 70 K, such scattering does not contribute significantly to the change in electrical conductivity because the motion of phonons is suppressed at this temperature.[3] Single crystal metals generally have a uniform surface orientation and relatively flat surfaces compared to polycrystalline metals. These surface properties are especially important for the heteroepitaxial growth of other materials such as thin films and in catalysis for various chemical reactions at the surface.

Single crystal metals are prepared by methods that can be classified in terms of phase transformations: liquid-solid (from melts or solutions), vapor-solid, or solid-solid. In the next three sections, we briefly describe growth from melts, epitaxial deposition in vapors and solutions, and abnormal grain growth in solids for the preparation of single crystal metals. We shall not cover chemical synthesis routes for intermetallic compounds with a well-defined stoichiometry. We also compare the preparation methods for single crystal metals and their shape-dependent uses ("bulk" vs "film and foil").

In particular, we focus on large-area single crystal metal "foils" that have been intensively studied during the past few years and consider their potential uses.

## GROWTH OF SINGLE CRYSTAL METALS FROM MELTS

Conventional methods for preparing single crystal metals are based on liquid-solid phase transitions. When a large volume of molten metal is supercooled, multiple nuclei are formed at the same time by homogeneous nucleation, yielding a polycrystalline product. A seed crystal having a specific crystallographic orientation and of the same metal is typically used for inhomogeneous nucleation, and a crystal having the same orientation as the seed can be grown from the melt.[4] The Czochralski and Bridgman methods are generally used to make bulk single crystals in large quantities.[5]

In a typical Czochralski process, a seed attached to a rod is "lowered" into contact with the molten metal contained in a crucible, and the rod is then slowly pulled out from the melt, yielding a single crystal by solidification.[3,6] During single crystal growth, the crystal is rotated for better heat and mass transport, yielding a large crystal with a cylindrical ingot shape [Figs. 1(a) and 1(b)].[3] The rotation and pulling processes in the Czochralski method are precisely controlled to get a high quality crystal.

The Bridgman method is simpler than the Czochralski method because it is not based on mass transport, only heat transport. In addition, the heat transport is more easily controlled by using a furnace rather than the complex rotation and pulling processes as in the Czochralski method. A container or a mold filled with the metal is passed through a furnace, which imposes a temperature gradient to produce a single crystal from the melt by unidirectional solidification from one end to the other.[7,8] By adjusting the shape of the container or mold, the shape of the single crystal product can be controlled [Figs. 1(c) and 1(d)].[7] In the Bridgman method, because nuclei are generated by supercooling of the melt at the liquid-solid interface, the crystal growth rate from these nuclei in the initial stage is very fast, resulting in the formation of a single crystal with many defects or a polycrystal in the presence of multiple nuclei. These problems can be overcome by remelting some of the nucleated crystals or by controlling the mold design (a conical end to generate a nucleus at one point or a small channel to allow only one nucleus having a fast growing crystallographic orientation to pass into the melt).[9] The most ideal solution for the supercooling and nucleation problems is the use of a single crystal seed. A better-quality single crystal can be obtained when a seed crystal is used. However, even though a seed crystal is used, single crystal metals produced by the Bridgman method are typically of lower quality than those produced by the Czochralski method because the melt and the growing crystal are in contact with the container so that the container material may be included as an impurity on the edge of the crystal. In addition, the orientation of the crystal may deviate because of unintended nucleation by the container or stress caused by the difference in thermal expansion between the container and the crystal during growth.

## EPITAXIAL DEPOSITION IN VAPORS AND SOLUTIONS

Single crystal metals can be produced by epitaxial deposition from vapors or solutions onto substrates, which act as seed layers. A single crystal metal produced by epitaxial deposition can be a film on a substrate or a foil if the film is in some way detached from the substrate.[10–12] Perhaps the simplest method to prepare single crystal metals through vapor-solid phase transformation is physical vapor deposition (PVD). The metal to be deposited as a thin film is vaporized and transported through a vacuum or using inert carrier gases. Typical examples are molecular beam epitaxy (MBE)[13–15] and sputtering.[16–24] In general, MBE can produce a higher quality epitaxial film than sputtering because it is performed under ultrahigh vacuum (UHV, $10^{-9}$–$10^{-10}$ Torr)[13–15] conditions, while sputtering is performed under relatively high pressure ($10^{-2}$–$10^{-3}$ Torr)[17–22] conditions that cause possible oxidation of the metal. In addition, the metal species that reach a substrate by sputtering have a much higher

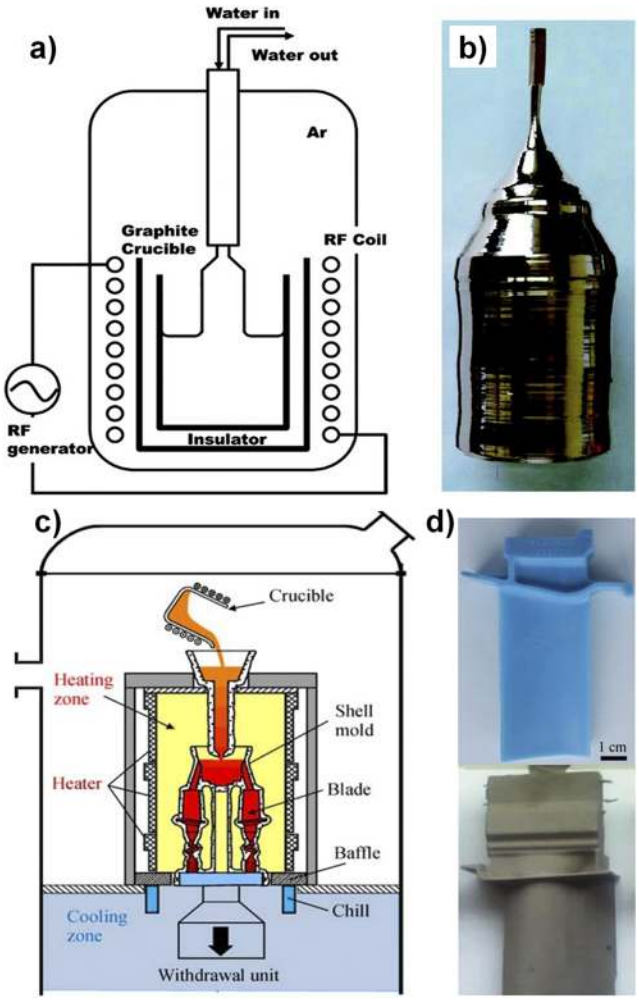


**FIG. 1**. (a) Schematic of the Czochralski method and (b) photograph of a single crystal Cu ingot made by the Czochralski method. Reprinted with permission from Cho *et al.*, Cryst. Growth Des. **10**, 2780–2784 (2010). Copyright 2010 American Chemical Society. (c) Schematic of the Bridgman method for shaped crystals and (d) photographs of a wax model for the mold preparation (top) and a Ni-based single crystal superalloy blade (CMSX-6 containing 10.0 wt. % Cr, 5.0 wt. % Co, 6.0 wt. % Ta, and other minor elements less than 5 wt. %) made from the mold. Reprinted with permission from D. Ma, Front. Mech. Eng. **13**, 3 (2018). Copyright 2018 Author(s), licensed under a Creative Commons Attribution 4.0 IPL License.

energy due to ionization than the thermally evaporated metal species in MBE. Uniform epitaxial deposition of metals can be obtained by MBE closer to the thermal equilibrium condition, while sputtering often produces relatively low quality films (e.g., rough surfaces or the presence of polycrystalline regions) due to their difficulty in controlling the metal clusters formed on the substrate. The growth of high-quality single crystal metal films using a single crystal metal as the sputtering target has been recently reported. The authors proposed that a single crystal target can produce more uniform as-sputtered metal clusters in terms of size and kinetic energy compared to a polycrystalline target, resulting in homogeneous crystal growth on the substrate.[19,20]

Epitaxial deposition of single crystal metals can also be achieved through solution processes, such as by electrodeposition onto metallic[12] or semiconducting substrates,[10,25,26] and insulating substrates with metallic buffer layers.[11] These approaches are generally less costly than vapor phase methods, but it is necessary to consider other factors, e.g., change in film morphology depending on the potential, the change in potential during deposition of metals, the chemisorption of anions, and the evolution of hydrogen gas to obtain high-quality single crystal metals.[27]

Single crystal substrates that are atomically flat with few defects and free of any adsorbents such as oxygen and water are preferable for the epitaxial deposition of single crystal metal films. The lattice mismatch between the deposited metal and the single crystal substrate is an important factor that determines the epitaxial growth. The lattice mismatch is defined as $(d_{\text{epitaxial layer}} - d_{\text{substrate}})/d_{substrate}$, where $d$ is the in-plane lattice constant. If the lattice mismatch is large, an epitaxial metal film can be under an unsustainable interfacial stress so that epitaxy is not achieved. However, epitaxial deposition can be achieved despite a large lattice mismatch by forming a "coincidence site lattice" between a metal and a substrate. For example, it has been reported that although Si(111) and Au(111) have a lattice mismatch of −24.9%, Au (111) can be epitaxially deposited on Si(111) because 4 unit meshes of Au and 3 unit meshes of Si form a coincidence site lattice (+0.1%).[10,25] Epitaxy can be classified into three growth modes according to the combination of the deposited metal and the single crystal substrate: layer-by-layer growth (Frank-van der Merwe mode), 3D island growth (Volmer-Weber mode), or island growth after layer growth (Stranski-Krastonov mode). In general, when the lattice mismatch between the single crystal substrate and the metal film with a particular surface orientation is small (e.g., homoepitaxy or near zero misfit), a pseudomorphic layer with respect to the orientation of the substrate can grow via the Frank-van der Merwe mode. If the lattice mismatch is relatively large, a film can grow by the Volmer-Weber mode. 3D islands are nucleated first and grown to eventually form a continuous film by coalescence of these islands. The Stranski-Krastonov mode is the intermediate between the Frank-van der Merwe and Volmer-Weber modes. In the Stranski-Krastonov mode, a film grows layer-by-layer in the initial stage, but above a critical thickness, misfit dislocations or undulations are created at the surface to relieve the stress accumulated by lattice mismatch. This changes the growth mode to the Volmer-Weber mode. In many cases of depositing a metal on a dielectric substrate, a film can grow by the Volmer-Weber mode.[28,29] For Volmer-Weber epitaxy, all isolated 3D nuclei must have the same orientation with an epitaxial relationship with the substrate. The deposition temperature (at the substrate) is a very important factor in obtaining these epitaxially oriented nuclei. The deposited metal clusters must grow above a critical size in order to act as nuclei with an epitaxial relationship with the substrate. In general, at low temperatures, since the adsorption rate of the metal vapor is faster than the lateral growth rate of the adsorbed metals, relatively low-quality or polycrystalline films consisting of very small metal clusters are formed. In contrast, at high temperatures, a smaller number of nuclei grow to a relatively larger size, and epitaxially oriented high crystallinity films can be obtained.[16,18,19,23] However, if the temperature is too high, the 3D islands can grow in the vertical (e.g., whiskers or rod shape) rather than in the lateral direction, resulting in a discontinuous film.[7,28] In addition, other contributions such as surface/interface energy and strain arising from the interface between the metal and the substrate should be taken into account at high temperature, which in some situations prevents epitaxial growth.[13,28] It is therefore important to find the optimum temperature range for each metal and substrate.[7,19,30] In order to improve the quality of deposited metal films (e.g., oxide removal and rearrangement of nonepitaxially deposited metal islands at low temperature), annealing at high temperatures after deposition is sometimes done.[16,17,21,24] This process is called "epitaxial grain growth." This postannealing minimizes the total energy of the film, which consists of the free surface energy of the films and the interfacial energy between the film and the substrate.

The dominantly oriented grains in the film are determined by the compromise of minimizing free surface energy and minimizing interfacial energy. If the contribution of the interfacial energy to the total reduction in energy during epitaxial grain growth is large, the final orientation of the film may have an epitaxial relationship with the substrate. Otherwise, sometimes a different film orientation compared to the film grown by conventional epitaxy is obtained.[28] This is related to abnormal grain growth in which only a few grains with a specific orientation with a low energy grow preferentially. Abnormal grain growth will be discussed in more detail in the next section.

Epitaxial deposition often results in the formation of a metal film with twin orientations on a single crystal substrate. For example, when 3-fold rotational symmetry metals such as Cu(111) are deposited on 6-fold rotational symmetry substrates such as α-$Al_2O_3$(0001), the deposited (epitaxial) metal can have two different orientations with a twin relationship.[14,17–19,21] The formation of these twin boundaries can be suppressed by modifying the interface between the metal and substrate (e.g., by the introduction of a thin buffer/seed layer[22] and/or chemical functionalization at the interface[21]) or by depositing the metal at high temperatures.[16,18] Increasing the adhesion between the metal and substrate by interfacial modification or deposition of the metals at high temperature promotes lateral growth of metal clusters, thereby reducing the probability of grains forming with different orientations. In a similar manner, there are reports that postannealing also can eliminate these twin orientated grains by the selective growth of a few grains that consume these twin oriented grains.[16,21]

## CONVERSION OF POLYCRYSTALLINE TO SINGLE CRYSTAL METALS BY ABNORMAL GRAIN GROWTH

GBs present in polycrystalline metals are, in most cases, thermodynamically unstable and should disappear if not for the sluggish

kinetics of the process. For metals at temperatures very low relative to their melting point, this does not happen (kinetically limited) because the rate of atomic diffusion in metals is slow. If metals are annealed at high temperatures where a relatively rapid diffusion of their atoms is possible, atoms can rearrange to form the lower energy configuration. Grain growth is a process in which grains grow in a polycrystalline solid at high temperature, removing GBs and lowering the energy of the crystalline solid. If grains grow uniformly over the entire sample, it is said to have a monodisperse size distribution of grains. If grain growth occurs inhomogeneously, i.e., with only a few grains growing relatively large, a bimodal size distribution of grains is seen. The former is called "normal grain growth" and the latter "abnormal grain growth."

In particular, abnormal grain growth is the key to producing single crystal metals through the growth of grains. If a limited number of grains in a polycrystalline matrix grow selectively and reach a size similar to that of the entire sample, the conversion of the polycrystalline metal into a single crystal is achieved. In normal grain growth, especially for thin films or foils, the maximum size of the (grown) grains is strongly related to the thickness of the sample. When the grain size is much smaller than the thickness, the grains can grow rapidly in a three-dimensional manner that is mainly driven by the curvature of the GBs. If the grains grow and eventually form a columnar grain structure where the size of the grains reaches the thickness of the sample, the growth of the grain is limited to one direction and the driving force for grain growth decreases. The development of thermal grooves where the GBs intersect the free surface, which happens as a result of equilibrium between surface tension and GB tension in columnar grain metals, can also limit the motion of GBs, resulting in termination of grain growth. In general, the maximum grain size that can be realized in normal grain growth is usually two or three times the thickness of the sample.[31] In order to grow grains much larger than the thickness of the sample and reach its lateral dimensions (millimeter or centimeter scale, or larger), normal grain growth must be prevented so that abnormal grain growth can occur. Abnormal grain growth is known to occur as a result of factors such as strain,[5,32–37] surface energy,[38–42] texture,[42,43] and second-phase precipitates,[44–46] when polycrystalline metals are annealed above their recrystallization temperatures. For example, a strongly textured metal is composed of grains with similar orientations and inevitably has a large fraction of low angle grain boundaries of low energy so that the driving force for normal grain growth is lower. If a new grain with a completely different orientation appears, it can form high angle grain boundaries of high energy, resulting in its abnormal growth.[31,42] Below, we will discuss the conversion of polycrystalline metals into single crystals by abnormal grain growth, when mainly driven by strain and surface energies.

The oldest and best-known method of preparing a single crystal metal through abnormal grain growth is critical strain annealing [Fig. 2(a)],[5,32,33] which generally consists of three steps: (1) briefly annealing a polycrystalline metal above the recrystallization temperature to remove residual stress in the sample, (2) straining the sample by a slight plastic deformation, (3) final annealing at a temperature that is typically higher than the first (brief) annealing. The

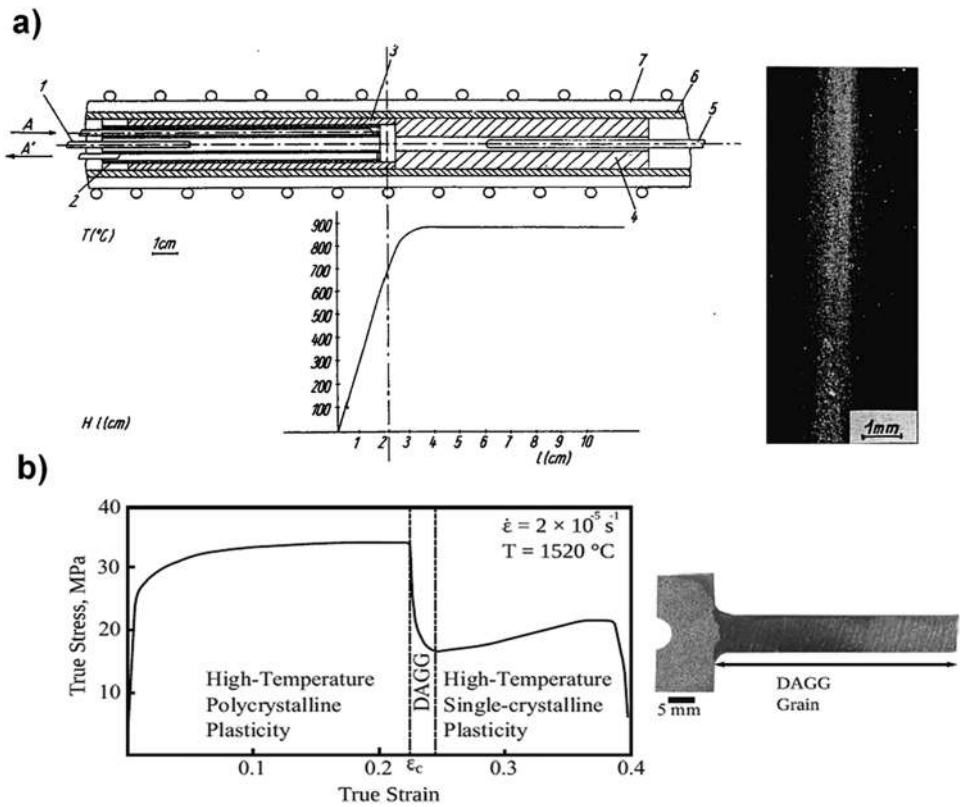


**FIG. 2**. (a) (Left) Schematic of the temperature gradient furnace and its annealing temperature profile and (right) photograph of a single crystal iron rod made by critical strain annealing. Adapted with permission from S. Kadeckov and B. Sestak Cryst. Res. Technol. **2**, 191 (1967). Copyright 2006 John Wiley and Sons. (b) (Left) Stress-strain curve of a Mo sheet and (right) photograph of a single crystal Mo sheet made by plastic deformation at high temperature. Reprinted with permission from P. J. Noell and E. M. Taleff, JOM **67**, 2642 (2015). Copyright 2015 Springer Nature.

key step in this process is the introduction of a small amount of strain that generates a limited number of nuclei and drives their growth during the final annealing. If the strain reaches a critical level, it can result in the polycrystalline metal growing into a single crystal during the final annealing, due to grain growth from a limited number of nuclei. In addition, straining by plastic deformation increases the dislocation density in the grains and enables them to grow faster and larger. If the strain is much lower or higher than this critical level, it can result in a polycrystalline metal due to no remarkable grain growth or grain growth from a large number of nuclei, at lower and higher strains than the critical level, respectively. A furnace with a temperature gradient is used to directionally grow the grain from one nucleus, and this has been found to increase the yield of single crystal metal. It has also been reported that single crystal metals can be obtained by applying plastic deformation during annealing because *in situ* straining can promote the motion of GBs, thereby resulting in abnormal grain growth [Fig. 2(b)].[34–36] Methods using this approach usually prepare single crystal metals in the form of a bar, sheet, or a wire. The preparation of complicated crystal shapes is rather challenging, since inhomogeneous plastic deformation in samples with complex shapes can cause fracture.

Achieving single crystal metal foils by abnormal grain growth has been intensively studied only in the past few years. All grain growth is basically related to the rearrangement of atoms into a lower energy configuration when atoms diffuse at a high temperature. Abnormal grain growth in thin foils is driven by minimizing the surface energy due to their shape because they have a larger surface to volume ratio than other forms of the metal. For example, when a face centered cubic (fcc) metal foil is annealed at a high temperature, abnormal growth of a grain having a {111} surface can occur resulting in single crystal metal foils.[39–42] Because the {111} surface has the lowest surface energy of all fcc surfaces,[47–49] a grain with {111} surface has a growth advantage over other grain orientations. However, if a metal foil is annealed when strongly attached to a substrate, similar to the case of a deposited metal on a substrate, the interfacial stress between the foil and substrate increases, which affects grain growth in the foil. The presence of these interfacial stresses in thin foils can cause the growth of grains with surface orientations other than those with a lower surface energy,[50,51] or they can prevent the growth of a large grain with a {111} surface, thereby resulting in polycrystalline foils.[42] In order to minimize such a stress from interfacial contact, we recently invented "contact-free annealing," in which the foil is freely suspended in certain gas atmospheres (for example, hydrogen) while being annealed (Fig. 3). Using this method, we can reproducibly convert commercial polycrystalline metal foils into single crystal metal foils for (to date) Cu, Ni, Pt, Co, and Pd with the surface orientations having the lowest energy.[42] In addition, we have taken the thus-produced single crystal Cu(111) foil and electroplated various amounts of Ni on both sides and then

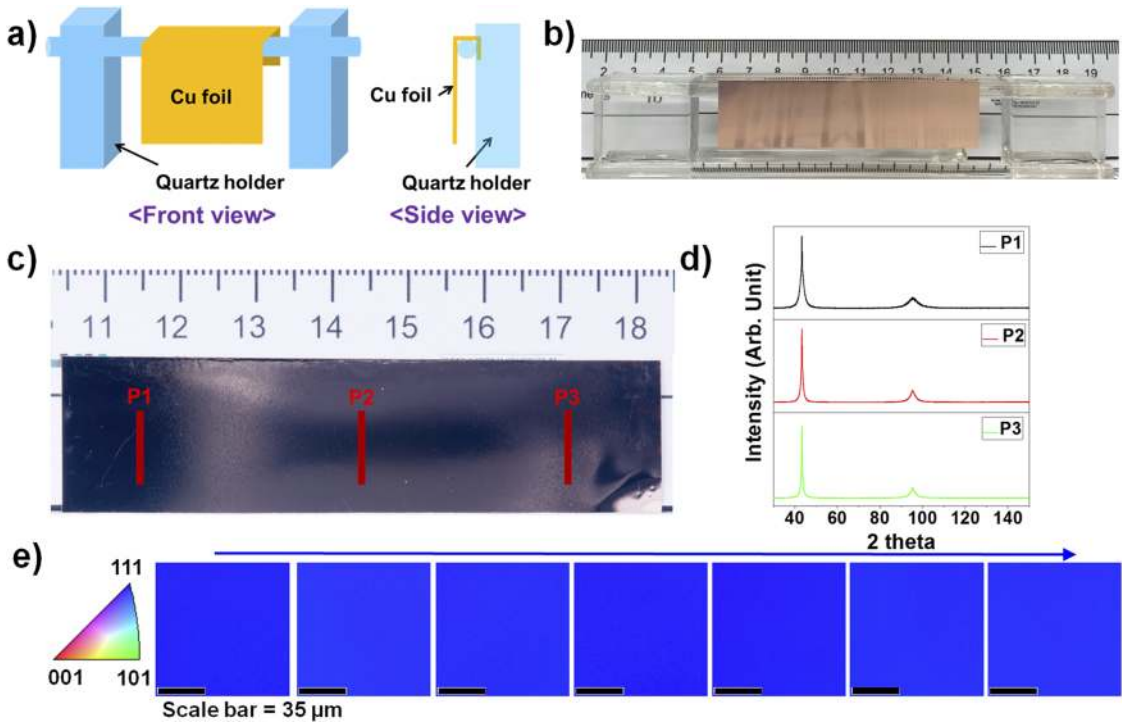


**FIG. 3**. (a) Schematic of the quartz holder from which the Cu foil is suspended and (b) photograph of the holder with the foil schematically shown in (a). (c) Photograph of the annealed single crystal Cu foil (the rulers in the photographs are centimeter scale), (d) X-ray diffraction (XRD) 2θ scans of the three regions in the annealed single crystal Cu foil indicated by P1-P3 in (c), and (e) Electron back scattered diffraction (EBSD) inverse pole figure (IPF) maps in the normal direction. Reprinted with permission from Jin *et al.*, Science **362**, 1021 (2018). Copyright 2018 The American Association for the Advancement of Science.

annealed such samples to generate single crystal Cu/Ni(111) foils, with fine tuning of the Ni concentration possible.[52]

The final orientation of the foil after abnormal grain growth is highly affected by the texture of the initial or intermediate stages of the annealing of the foil. For example, we observed that cold rolled Cu foils with a strong {112} ⟨111⟩ texture in the early and intermediate stages of annealing can be converted into single crystal foils with {111} ⟨112⟩ texture by abnormal grain growth. This occurs by the abnormal growth of {111} ⟨112⟩ orientated grains formed in the final stage of annealing. Such a {111} ⟨112⟩ grain with the lowest surface energy grows larger by consuming {112} ⟨111⟩ oriented grains with a relatively higher energy. On the other hand, other cold rolled-Cu foils having strong {112} ⟨111⟩ but also additional {100} ⟨001⟩ textures show a different final orientation after abnormal grain growth. In the intermediate stage of annealing, the initial {100} ⟨001⟩ texture, which is relatively lower in energy than {112} ⟨111⟩, developed so that the {112} ⟨111⟩ texture disappeared. Then, this {100} ⟨001⟩ texture in the intermediate stage consequently resulted in centimeter-scale grains close to the {100} surface orientation.[42] In general, according to manufacturing history, commercial metal foils can have different initial textures that result in different orientations after annealing.

The gas atmosphere (composition, pressure) can be an important factor for the conversion to single crystal metal foils. In particular, the presence or absence of $H_2$ gas during annealing influences the conversion into single crystal metals. Hydrogen penetrates all metals and in many stabilizes vacancies, thus increasing their equilibrium concentration. This increased vacancy concentration can promote the rearrangement of metal atoms during annealing, possibly enhancing conversion into a single crystal metal foil. For example, we have reported that polycrystalline Cu, Ni, and Co foils cannot be converted to single crystals during annealing in the presence of Ar without hydrogen, and single crystal Cu(111), Ni(111), and Co(0001) foils were only obtained during annealing with mixtures of $H_2$ and Ar gases. On the other hand, single crystal Pt(111) foils were obtained during annealing with but also without hydrogen, due to the much higher vacancy concentration in Pt than in the three other metals at the annealing temperature we used.[42] It was reported that single crystal Cu(001) foils were obtained by preoxidation of a polycrystalline Cu foil in a hydrogen-free atmosphere followed by sequential reductions under $H_2$ gas at high temperature.[53] It was claimed that the surface of the Cu was oxidized during high temperature annealing (e.g., over 1000 °C) in a hydrogen free atmosphere by the presence of trace amounts of oxygen in the furnace and the surface oxide layers stabilized the {001} surface orientation rather than the {111} surface orientation, thereby resulting in single crystal Cu(001) foils or {001} textured foils.[53,54]

## COMPARISON OF DIFFERENT PREPARATION METHODS OF SINGLE CRYSTAL METALS AND THEIR SHAPE-DEPENDENT USES ("BULK" VS "FILM AND FOIL")

We have discussed growth from melts, epitaxial deposition in vapors and solids, and abnormal grain growth in solids for the preparations of single crystal metals. Each growth method has different advantages and disadvantages, and the uses of single crystal metals can depend on the shape produced.

The methods to grow single crystal metals from melts require a high temperature to melt the metal, and the process of growing the single crystal by solidifying the melt needs to be carefully controlled, which means that a relatively large investment for equipment is required. Therefore, single crystal metals prepared by these methods are relatively expensive. As an example, a commercial single crystal Cu plate made by the Czochralski method currently costs over $ 150 per square centimeter (for a typical thickness of 1 mm and a purity of 99.99 wt. %, one side polished). Compared to that of a polycrystalline Cu plate with the exactly same specifications (about $ 30 per square centimeter), it is obvious that considerable cost is involved in the manufacture of the former. The epitaxial deposition of metals onto a single crystal substrate to generate single crystal films is less expensive and typically simpler than growth from the melt. Of course, this method calls for a single crystal ("wafer") substrate, and the size of the single crystal film is thus limited by the size of the single crystal substrate. Abnormal grain growth in solids to generate single crystal metal samples has the advantage of being relatively inexpensive, because it involves the conversion of commercially available polycrystalline metal samples into single crystals. For example, a polycrystalline Cu foil with a thickness of 80 $\mu$m and a purity of 99.9 wt. % can be converted to a single crystal and costs less than $ 0.05 per square centimeter.[52] If process optimization for mass production is done, there is a possibility that large area single crystal metals (cm scale or more) can be obtained at a very low cost.[41,42,55]

The growth of single crystal metals from melts is used for the mass production of bulk single crystals, the most typical of which are single crystal superalloys. Particularly, examples are Ni-based superalloys, for example, Mar-M200 (9.0 wt. % Cr, 10.0 wt. % Co, 12.5 wt. % W) and Hastelloy X (22.0 wt. % Cr, 9.0 wt. % Mo, 18.5 wt. % Fe, with the balance being Ni). Other minor elements are present in both these superalloys, but each of these constitutes less than 5 wt. %. These have been widely used as turbine blade materials in aircraft and in gas and steam engines.[7,56–58] Turbine blades are generally exposed to high temperature and pressure conditions for extended periods of time, and under these conditions, even stress that is below the yield stress may accumulate over time, eventually causing plastic deformation of the material, i.e., "creep". Creep is caused by the sliding of GBs that can result in the intergranular fracture of materials, and in a turbine blade, it occurs mainly at GBs perpendicular to the stress axis, so that making turbine blades with a columnar grain structure aligned along the stress axis is a way to avoid this. The use of single crystal metals without GBs as turbine blade materials is more effective than using unidirectional columnar structured metals to reduce the creep behavior (Table I).[7,56–58]

Because bulk single crystal metals are generally produced in large ingots, they must be cut into smaller pieces and their cut surfaces polished if necessary for practical uses. They are mainly processed into sheets or bars, and have been used to study the intrinsic properties of single crystals and also as substrates for fundamental scientific studies such as in surface science. Because polycrystalline metals consist of numerous crystal grains, it is typically not possible to measure the properties of a selected grain and GB. The properties of a crystallographic grain can be measured by using single crystal samples having the same orientation as it. Studying the properties of single crystal metals can also be of great help in predicting

**TABLE I**. Creep and stress-rupture properties of the Ni-based superalloy Mar-M200. Adapted with permission from F. I. Versnyder and M. E. Shank, Mater. Sci. Eng. **6**, 213 (1970). Copyright 1970 Elsevier.

| | 1400 °F/100 k.s.i | | 1600 °F/50 k.s.i | | 1800 °F/30 k.s.i | |
|---|---|---|---|---|---|---|
| | Rupture life (h) | Min. creep rate (in./in./h) | Rupture life (h) | Min. creep rate (in./in./h) | Rupture life (h) | Min. creep rate (in./in./h) |
| Equiaxed grains | 4.9 | $70.0 \times 10^{-5}$ | 245.9 | $3.4 \times 10^{-5}$ | 35.6 | $23.8 \times 10^{-5}$ |
| Unidirectional columnar grains | 366.0 | $14.5 \times 10^{-5}$ | 280.0 | $7.7 \times 10^{-5}$ | 67.0 | $25.6 \times 10^{-5}$ |
| Single crystal | 1914.0 | $2.2 \times 10^{-5}$ | 848.0 | $1.4 \times 10^{-5}$ | 107.0 | $16.1 \times 10^{-5}$ |

the properties of their polycrystalline counterparts. For example, if there are data on the mechanical properties of grains obtained from single crystal samples and the microstructural data of the polycrystalline metal such as the orientations of individual grains, the arrangement of grains, and dislocations, it is possible to estimate the mechanical properties of the polycrystalline metal to some extent.[59,60]

As model systems, single crystal metal surfaces are critical to obtain a fundamental understanding of catalysis and predicting the behavior of real catalysts. Various catalytic reactions such as the oxygen reduction reaction (ORR), carbon dioxide reduction reaction, carbon monoxide oxidation, hydrogenation/dehydrogenation of hydrocarbons, and the dissociation of molecules on catalytic surfaces of single crystal metals such as Pt, Pd, Ag, and Cu have been studied in terms of the reaction rate, the catalytic activity and absorbed reactants and products.[61–65] For example, the ORR activity of single crystal Pt is highly dependent on its crystallographic orientation [e.g., Pt(111) > Pt(211) > Pt(110) > Pt(100) in alkaline solutions], and the activity can also be affected by structures such as terraces and steps that are present on the surface of the crystal (e.g., the adsorption of O or OH species in ORR takes place first at the steps).[63] If the catalytic properties of different crystal planes are determined from single crystal metal surfaces used as model catalysts, the properties of real catalysts, even nanoparticles, which are composed of differently oriented facets and steps, can be predicted.[66,67]

As already mentioned, epitaxial film growth on single crystal substrates yields single crystal thin films, and abnormal grain growth can be used to prepare shapes, such as rods, bars, and more importantly, foils. For surface studies, single crystal samples have typically been obtained by cutting from expensive large bulk single crystals. The processes of slicing and then polishing to have a smooth surface also add to the cost of the process. In contrast, single crystal metal films and foils, especially those produced by high temperature annealing, can have an atomically flat surface (with sub-nm scale roughness in terrace regions over several tens of micrometers[19,20,24,42] and a roughness of a few nanometers even in relatively rough stepped regions[23,42]) without the need for any polishing. The essentially flat surfaces of single crystal metal films and foils allow them to be used in surface studies, especially as model catalysts. For example, the selectivity of the carbon dioxide reduction reaction on Cu(111), Cu(001), and Cu(751) single crystal films has been studied, and the Cu(751) film was reported to be the most selective.[65] However, using single crystal metal foils as model catalysts has not yet been reported since these have been intensively studied only in recent years, but recent studies on the local catalytic activity in the micrometer scale grains of polycrystalline Pt, Pd, and Rh foils by photoemission electron microscopy (PEEM) suggest that single crystal metal foils can also be used as model catalysts.[68]

Single crystal metal films and foils can serve as good substrates for the heteroepitaxial growth of other materials due to their uniform crystallographic orientation and flat surfaces. In particular, two-dimensional (2D) films such as graphene and hexagonal boron nitride (hBN) have been grown on such metal foils by chemical vapor deposition (CVD), and this process has been upscaled for producing large area films.[69] Both graphene and hBN have been grown on polycrystalline metal substrates by CVD, but as a result, they are polycrystalline, consisting of randomly oriented crystallites with GBs between them. GBs are known to degrade the mechanical and electrical properties of 2D materials,[70,71] and therefore, the growth of 2D materials without GBs is of great importance. Cu(111), Ni(111), and Co(0001) have small lattice mismatches with graphene of −3.4%, −1.2%, and −1.8%,[72,73] respectively, and have been found to be good substrates for the epitaxial growth of graphene [Fig. 4(a)]. Until now, most studies on the epitaxial growth of graphene on single metals have focused on Cu(111) substrates[17,18,20,22,24,39,40,74–76] since the low carbon solubility of Cu allows the formation of a uniform monolayer single crystal graphene through self-limited growth. It has been reported that graphene islands grown on Cu(111) or Cu/Ni(111) alloy foils have regular hexagonal shapes and are aligned in a particular direction due to their identical or similar crystal orientations.[39,40,42,52,74,75] When graphene islands with the same crystal orientation grow and coalesce, there is no GB formation,[40,52] resulting in single crystal graphene films [Fig. 4(b)]. Because of the absence of GBs, single crystal graphene grown on single crystal metal substrates was reported to have better mechanical and electrical properties compared with polycrystalline graphene grown on polycrystalline metal substrates (e.g., Young's modulus: 796 ± 63 and 733 ± 70 GPa, and hole mobility: $1.1 \times 10^4$ and $6.9 \times 10^3$ $cm^2/V$ s for single crystal and polycrystalline graphenes, respectively).[75,76] However, the growth of single crystal graphenes on single crystal metal substrates still has some issues that need to be addressed. One is the formation of parallel "folds," which are three-layer graphene regions that can have lengths of millimeters and widths from tens to hundreds of nanometers. Such folds are caused by the differential thermal contraction between the metal and the epitaxially grown graphene during cooling [Fig. 4(b)].[52,75,76] The elimination of such defects should further improve the performance of single crystal graphene.

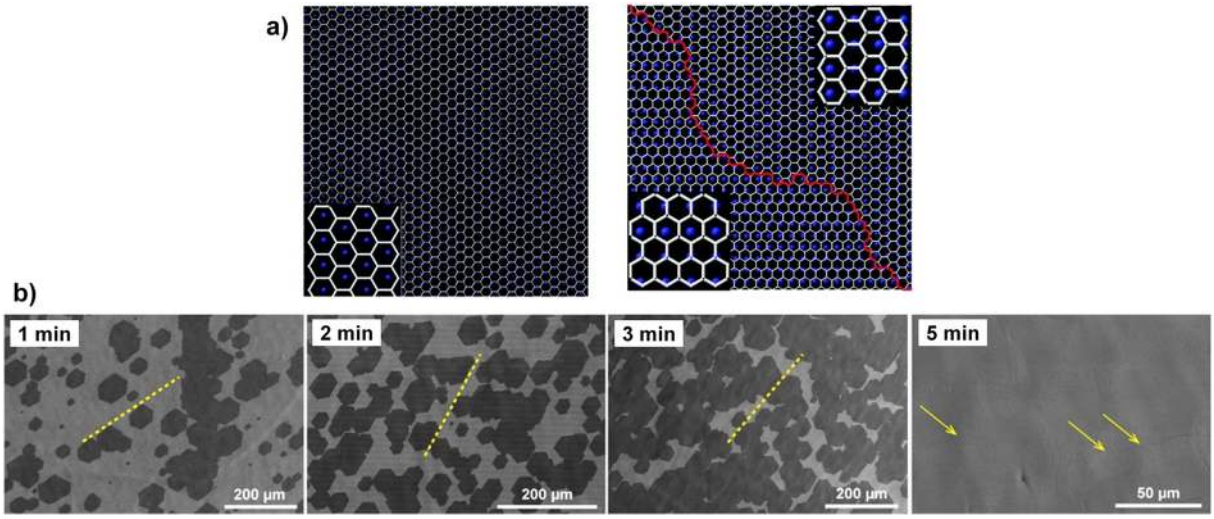


**FIG. 4**. (a) Atomic models of graphene grown on Cu(111) (left) and Cu(100) (right). The graphene grown on Cu(111) is a single crystal, while that grown on Cu(100) is polycrystalline due to the lattice mismatch between graphene and substrate. Reprinted with permission from Ogawa *et al.*, J. Phys. Chem. Lett. **3**, 219 (2012). Copyright 2012 American Chemical Society.[85] White lines are graphene and blue spheres are Cu atoms. (b) SEM images of graphene grown on Cu/Ni(111) alloy foils for different growth times. Graphene islands grow in alignment with each other, and due to their same orientation, join together to form single crystal graphene. Yellow lines indicate the alignment directions of the graphene islands and yellow arrows indicate folds in the graphene layer. Adapted with permission from Huang *et al.*, ACS Nano **12**, 6117 (2018). Copyright 2018 American Chemical Society.

hBN can also be grown epitaxially on single crystal metal substrates, such as Cu(111), Ni(111), and Co(0001), and because it has a lattice constant similar to graphene, it also has small lattice mismatch with these metals.[69] Epitaxial growth of aligned triangular hBN domains on Cu(111) foils has been reported;[77,78] however, domains with two different orientations were observed. Similar to the epitaxial deposition of Cu(111) on α-$Al_2O_3$(0001) discussed in the previous section, since hBN has 3-fold rotational symmetry, two different triangular domains having a twin relationship to each other can be grown on the topmost atom layer of a Cu(111) surface, which has a 6-fold rotational symmetry. When these antiparallel domains coalesce during growth, commensurate stitching does not occur and domain boundaries are formed.[77] To circumvent this problem, a recent study reported that the large area single crystal hBN film can be produced on a Cu(110) vicinal surface instead of a Cu(111) surface.[55] They claimed that the vicinal surface of Cu(110) has parallel steps in the ⟨211⟩ direction, and coupling between these step edges and hBN zigzag edges can cause the unidirectional growth of hBN domains, resulting in a single crystal hBN film. This suggests that single crystal metal substrates, when appropriately processed, can be successfully used to grow various 2D materials even when there is a large lattice mismatch between the substrate and the grown material.

## FUTURE PERSPECTIVES

In this section, we briefly consider a few potential applications of large-area single crystal metal foils. However, we expect that as such foils become readily available, many creative ways to use them will be found.

Due to the absence of GBs that cause electron scattering and decrease electrical conductivity, metal single crystals have a higher electrical conductivity than their polycrystalline counterparts.[79] For example, the room temperature electrical conductivity is around 7% higher for a single crystal Cu(111) foil when compared to polycrystalline Cu [Fig. 5(a)].[42] Similarly, a ~9% higher room temperature electrical conductivity was reported for a single crystal Cu wire made from Czochralski-grown single crystal Cu, when compared to a polycrystalline Cu wire.[3] Thus, single crystal metal foils can substitute for polycrystalline metals in many areas including electrically conductive wires or electrodes after proper processing to the desired shapes and could potentially lead to significant improvement in performance and energy saving. For example, a transparent and flexible organic light-emitting diode (OLED) has been reported by using a single crystal Au foil as an electrode, which showed a sheet resistance of 7 Ω/sq with 25% transmittance at 500 nm wavelength and only a 4% increase of resistance even after 4000 bending cycles. In addition, an epitaxially grown $Cu_2O$ semiconductor on such Au foil showed better efficiency with a diode quality factor of 1.6, compared to a polycrystalline $Cu_2O$ diode with a diode factor of 3.1 due to reducing the possible electron-hole recombination at GBs (an ideal diode factor is 1.0) [Fig. 5(b)].[10]

Another potential application of single crystal metal foils is in the field of high temperature superconductors (HTSs). Single crystal metal foils might be used as substrates for the growth of second-generation (2G) high temperature superconducting in the form of a large area thin film that could be processed to form wires. $YBa_2Cu_3O_{7-\delta}$ (YBCO) is widely used as the superconducting material in 2G HTS to enable a high current-carrying capacity, which is dependent on the degree of orientation of the YBCO layers. The rolling-assisted biaxially textured substrate (RABiTS) method has been used to grow biaxially textured large-area YBCO at low cost. In this method, the texture of the metal (usually a Ni- or Cu-based

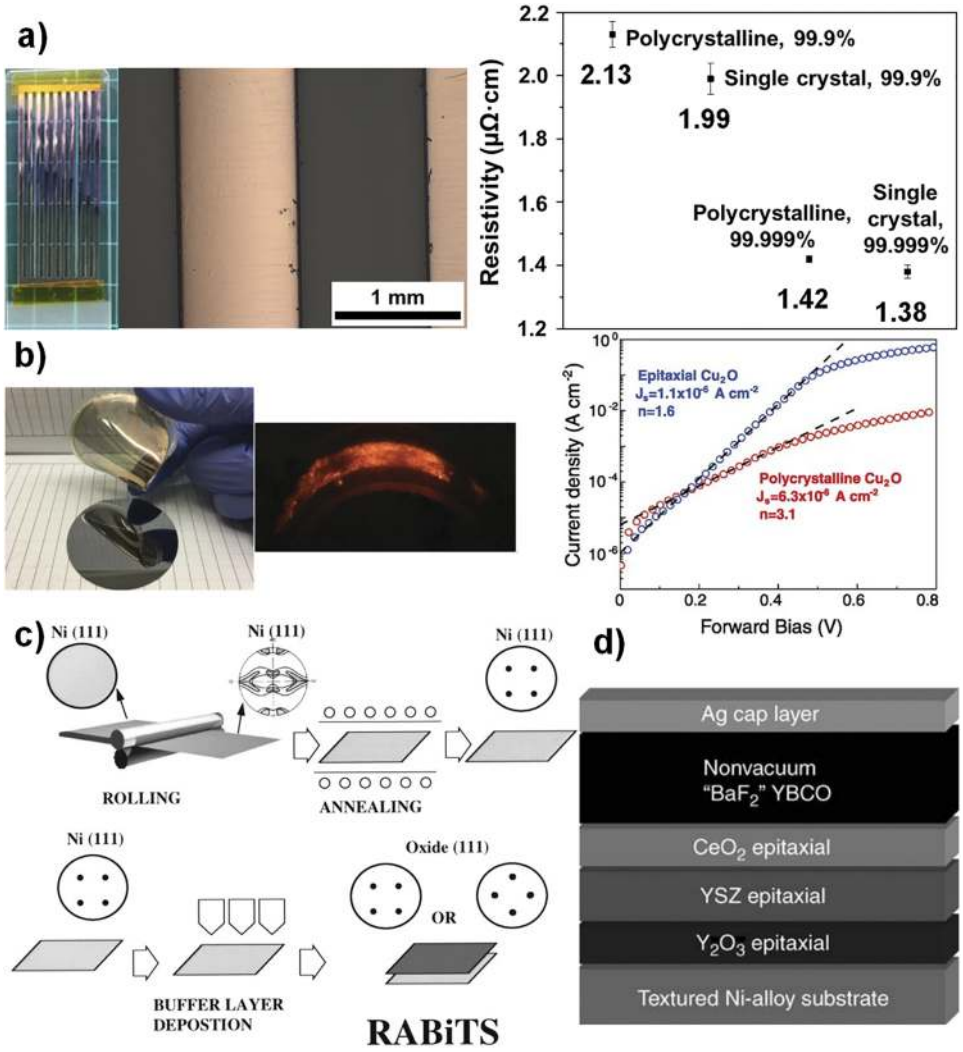


**FIG. 5**. (a) (Left) Photograph and optical microscope image of Cu strips made from Cu foils, and (right) resistivity of the as-received and single crystal Cu foils with 99.9% and 99.999% purities. Adapted with permission from Jin *et al.*, Science **362**, 1021 (2018). Copyright 2018 The American Association for the Advancement of Science. (b) (Left) Photograph of a 28 nm-thick transparent and flexible single crystal Au foil, (middle) an OLED device made on this foil, and (right) dark saturation current density and diode quality factor of epitaxial and polycrystalline $Cu_2O$ diodes. Adapted with permission from Mahenderkar *et al.*, Science **355**, 1203 (2017). Copyright 2017 The American Association for the Advancement of Science. (c) Schematic of the Rolling-assisted biaxially textured substrates (RABiTS) process: a randomly oriented Ni plate is converted to a copper-type textured Ni foil by cold rolling. It is then converted to the cube textured (a kind of biaxial texture) Ni foil by annealing. Finally, the metal and/or oxide buffer layer(s) are epitaxially deposited onto the biaxially textured Ni foil for the deposition of YBCO [the (111) pole figures of the insets represent textures in each step]. Reprinted with permission from Goyal *et al.*, Appl. Supercond. **4**, 403 (1996). Copyright 1996 Elsevier. (d) Schematic structure of 2G HTS using a RABiTS. Reprinted with permission from Goyal *et al.*, MRS Bull. **29**, 552 (2004). Copyright 2011 Cambridge University Press.

alloy) foils is controlled by cold rolling and recrystallization to obtain a biaxial texture. A layer of YBCO layer is then "epitaxially" deposited on the metal foil (after the sequential deposition of buffer layers) to achieve a biaxially textured 2G HTS [Figs. 5(c) and 5(d)].[80–84] In superconducting materials, the current loss at the GBs is related to their misorientation angles. Polycrystalline materials with random grain orientations mainly consist of high angle boundaries (with a misorientation angle between grains >5°), and therefore have a more disordered structure than those with low angle boundaries (misorientation angle between grains <5°) and, consequently, high losses occur when current passes through these disordered boundaries. On the other hand, biaxially textured materials are composed of grains with similar orientations with a high fraction of low angle boundaries and can therefore carry higher current than randomly oriented polycrystalline materials.[84] If large area single crystal metal foils are used as the substrate instead of biaxially textured foils, epitaxial deposition of YBCO layers with an almost single crystal orientation with the absence of GBs might be achieved, perhaps resulting in a higher current carrying capacity than the HTS made from biaxially textured metal foils.

We repeat that the main advantage of single crystal metal foils is in the production of a *large area* single crystal foils by a process that is relatively inexpensive. Many other uses will be discovered and identified as scientists and engineers use such foils.

## ACKNOWLEDGMENTS

This work was supported by IBS-R019-D1. We appreciate the reviewers' insightful and helpful comments on our manuscript.

## REFERENCES

[1] P. W. Bridgman, Proc. Natl. Acad. Sci. U. S. A. **10**, 411 (1924).
[2] P. Salunke, M. Joshi, V. Chaswal, G. Q. Zhang, L. A. Rosenbaum, K. Dowling, P. Decker, and V. Shanov, Rev. Sci. Instrum. **87**, 105126 (2016).

[3]Y. C. Cho, S. Lee, M. Ajmal, W. K. Kim, C. R. Cho, S. Y. Jeong, J. H. Park, S. E. Park, S. Park, H. K. Pak, and H. C. Kim, Cryst. Growth Des. **10**, 2780–2784 (2010).
[4]K. Sato, Y. Furukawa, and K. Nakajima, *Advances in Crystal Growth Research*, 1st ed. (Elsevier Science B. V., Amsterdam, 2001).
[5]H. C. H. Carpenter, Nature **118**, 266 (1926).
[6]G. Dhanaraj, *Springer Handbook of Crystal Growth* (Springer-Verlag Berlin Heidelberg, Berlin, Heidelberg, 2010).
[7]H. Fredriksson and U. Akerlind, *Solidification and Crystallization Processing in Metals and Alloys* (John Wiley & Sons, Chichester, 2012).
[8]S. Kasap and P. Capper, *Springer Handbook of Electronic and Photonic Materials* (Springer International Publishing, Cham, 2017).
[9]B. R. Pamplin, *Crystal Growth: International Series on the Science of the Solid State*, 2nd ed. (Pergamon Press, Oxford, 1980).
[10]N. K. Mahenderkar, Q. Z. Chen, Y. C. Liu, A. R. Duchild, S. Hofheins, E. Chason, and J. A. Switzer, Science **355**, 1203 (2017).
[11]H. K. Yu, K. Balasubramanian, K. Kim, J. L. Lee, M. Maiti, C. Ropers, J. Krieg, K. Kern, and A. M. Wodtke, ACS Nano **8**, 8636 (2014).
[12]J. W. Shin, A. Standley, and E. Chason, Appl. Phys. Lett. **90**, 261909 (2007).
[13]G. Dehm, M. Ruhle, G. Ding, and R. Raj, Philos. Mag. B **71**(6), 1111–1124 (1995).
[14]D. L. Medlin, K. F. McCarty, R. Q. Hwang, S. E. Guthrie, and M. I. Baskes, Thin Solid Films **299**, 110 (1997).
[15]G. Dehm, C. Scheu, M. Ruhle, and R. Raj, Acta Mater. **46**, 759 (1998).
[16]D. L. Miller, M. W. Keller, J. M. Shaw, K. P. Rice, R. R. Keller, and K. M. Diederichsen, AIP Adv. **3**, 082105 (2013).
[17]B. S. Hu, H. Ago, Y. Ito, K. Kawahara, M. Tsuji, E. Magome, K. Sumitani, N. Mizuta, K. Ikeda, and S. Mizuno, Carbon **50**, 57 (2012).
[18]C. M. Orofeo, H. Hibino, K. Kawahara, Y. Ogawa, M. Tsuji, K. Ikeda, S. Mizuno, and H. Ago, Carbon **50**, 2189 (2012).
[19]S. H. Lee, J. Y. Kim, T. W. Lee, W. K. Kim, B. S. Kim, J. H. Park, J. S. Bae, Y. C. Cho, J. D. Kim, M. W. Oh, C. S. Hwang, and S. Y. Jeong, Sci. Rep. **4**, 6230 (2014).
[20]V. L. Nguyen, D. J. Perello, S. Lee, C. T. Nai, B. G. Shin, J. G. Kim, H. Y. Park, H. Y. Jeong, J. Zhao, Q. A. Vu, S. H. Lee, K. P. Loh, S. Y. Jeong, and Y. H. Lee, Adv. Mater. **28**, 8177 (2016).
[21]K. Verguts, B. Vermeulen, N. Vrancken, K. Schouteden, C. Van Haesendonck, C. Huyghebaert, M. Heyns, S. De Gendt, and S. Brems, J. Phys. Chem. C **120**, 297 (2016).
[22]D. L. Miller, M. W. Keller, J. M. Shaw, A. N. Chiaramonti, and R. R. Keller, J. Appl. Phys. **112**, 064317 (2012).
[23]T. Iwasaki, H. J. Park, M. Konuma, D. S. Lee, J. H. Smet, and U. Starke, Nano Lett. **11**, 79 (2011).
[24]H. Ago, Y. Ohta, H. Hibino, D. Yoshimura, R. Takizawa, Y. Uchida, M. Tsuji, T. Okajima, H. Mitani, and S. Mizuno, Chem. Mater. **27**, 5377 (2015).
[25]J. A. Switzer, J. C. Hill, N. K. Mahenderkar, and Y. C. Liu, ACS Appl. Mater. Interfaces **8**, 15828 (2016).
[26]P. Prod'homme, F. Maroun, R. Cortes, and P. Allongue, Appl. Phys. Lett. **93**, 171901 (2008).
[27]P. Allongue and F. Maroun, Curr. Opin. Solid State Mater. Sci. **10**, 173 (2006).
[28]C. V. Thompson, J. Floro, and H. I. Smith, J. Appl. Phys. **67**, 4099 (1990).
[29]S. C. Seel and C. V. Thompson, J. Appl. Phys. **93**, 9038 (2003).
[30]K. M. Reddy, A. D. Gledhill, C. H. Chen, J. M. Drexler, and N. P. Padture, Appl. Phys. Lett. **98**, 113117 (2011).
[31]F. J. Humphreys and M. Hatherly, *Recrystallization and Related Annealing Phenomena*, 2nd ed. (Elsevier Ltd., Oxford, 2004).
[32]H. C. H. Carpenter and C. F. Elam, Proc. R. Soc. A **100**, 329 (1921).
[33]S. Kadeckov and B. Sestak, Cryst. Res. Technol. **2**, 191 (1967).
[34]J. Ciulik and E. M. Taleff, Scr. Mater. **61**, 895 (2009).
[35]N. A. Pedrazas, T. E. Buchheit, E. A. Holm, and E. M. Taleff, Mater. Sci. Eng.: A **610**, 76 (2014).
[36]P. J. Noell and E. M. Taleff, JOM **67**, 2642 (2015).
[37]I. Jo, S. Park, D. Kim, J. S. Moon, W. B. Park, T. H. Kim, J. H. Kang, W. Lee, Y. Kim, D. N. Lee, S. P. Cho, H. Choi, I. Kang, J. H. Park, J. S. Lee, and B. H. Hong, 2D Mater. **5**, 024002 (2018).
[38]C. C. Wong, H. I. Smith, and C. V. Thompson, Appl. Phys. Lett. **48**, 335 (1986).
[39]L. Brown, E. B. Lochocki, J. Avila, C. J. Kim, Y. Ogawa, R. W. Havener, D. K. Kim, E. J. Monkman, D. E. Shai, H. F. I. Wei, M. P. Levendorf, M. Asensio, K. M. Shen, and J. Park, Nano Lett. **14**, 5706 (2014).
[40]V. L. Nguyen, B. G. Shin, D. L. Duong, S. T. Kim, D. Perello, Y. J. Lim, Q. H. Yuan, F. Ding, H. Y. Jeong, H. S. Shin, S. M. Lee, S. H. Chae, Q. A. Vu, S. H. Lee, and Y. H. Lee, Adv. Mater. **27**, 1376 (2015).
[41]X. Z. Xu, Z. H. Zhang, J. C. Dong, D. Yi, J. J. Niu, M. H. Wu, L. Lin, R. K. Yin, M. Q. Li, J. Y. Zhou, S. X. Wang, J. L. Sun, X. J. Duan, P. Gao, Y. Jiang, X. S. Wu, H. L. Peng, R. S. Ruoff, Z. F. Liu, D. P. Yu, E. G. Wang, F. Ding, and K. H. Liu, Sci. Bull. **62**, 1074 (2017).
[42]S. Jin, M. Huang, Y. Kwon, L. N. Zhang, B. W. Li, S. Oh, J. C. Dong, D. Luo, M. Biswal, B. V. Cunning, P. V. Bakharev, I. Moon, W. J. Yoo, D. C. Camacho-Mojica, Y. J. Kim, S. H. Lee, B. Wang, W. K. Seong, M. Saxena, F. Ding, H. J. Shin, and R. S. Ruoff, Science **362**, 1021 (2018).
[43]A. D. Rollett and W. W. Mullins, Scr. Mater. **36**, 975 (1997).
[44]A. Gangulee and F. M. Dheurle, Thin Solid Films **12**, 399 (1972).
[45]T. Omori, T. Kusama, S. Kawata, I. Ohnuma, Y. Sutou, Y. Araki, K. Ishida, and R. Kainuma, Science **341**, 1500 (2013).
[46]T. Kusama, T. Omori, T. Saito, S. Kise, T. Tanaka, Y. Araki, and R. Kainuma, Nat. Commun. **8**, 354 (2017).
[47]L. Vitos, A. V. Ruban, H. L. Skriver, and J. Kollar, Surf. Sci. **411**, 186 (1998).
[48]G. C. Kallinteris, N. I. Papanicolaou, G. A. Evangelakis, and D. A. Papaconstantopoulos, Phys. Rev. B **55**, 2150 (1997).
[49]Q. Jiang, H. M. Lu, and M. Zhao, J. Phys.: Condens. Matter **16**, 521 (2004).
[50]C. V. Thompson and R. Carel, J. Mech. Phys. Solids **44**, 657 (1996).
[51]J. Greiser, D. Muller, P. Mullner, C. V. Thompson, and E. Arzt, Scr. Mater. **41**, 709 (1999).
[52]M. Huang, M. Biswal, H. J. Park, S. Jin, D. Qu, S. Hong, Z. L. Zhu, L. Qiu, D. Luo, X. C. Liu, Z. Yang, Z. L. Liu, Y. Huang, H. Lim, W. J. Yoo, F. Ding, Y. L. Wang, Z. Lee, and R. S. Ruoff, ACS Nano **12**, 6117 (2018).
[53]H. Wang, X. Z. Xu, J. Y. Li, L. Lin, L. Z. Sun, X. Sun, S. L. Zhao, C. W. Tan, C. Chen, W. H. Dang, H. Y. Ren, J. C. Zhang, B. Deng, A. L. Koh, L. Liao, N. Kang, Y. L. Chen, H. Q. Xu, F. Ding, K. H. Liu, H. L. Peng, and Z. F. Liu, Adv. Mater. **28**, 8968 (2016).
[54]J. X. Hu, J. B. Xu, Y. F. Zhao, L. Shi, Q. Li, F. K. Liu, Z. Ullah, W. W. Li, Y. F. Guo, and L. W. Liu, Sci. Rep. **7**, 45358 (2017).
[55]L. Wang, X. Z. Xu, L. N. Zhang, R. X. Qiao, M. H. Wu, Z. C. Wang, S. Zhang, J. Liang, Z. H. Zhang, Z. B. Zhang, W. Chen, X. D. Xie, J. Y. Zong, Y. W. Shan, Y. Guo, M. Willinger, H. Wu, Q. Y. Li, W. L. Wang, P. Gao, S. W. Wu, Y. Zhang, Y. Jiang, D. P. Yu, E. G. Wang, X. D. Bai, Z. J. Wang, F. Ding, and K. H. Liu, Nature **570**, 91 (2019).
[56]F. I. Versnyder and M. E. Shank, Mater. Sci. Eng. **6**, 213 (1970).
[57]T. Nishinaga, *Handbook of Crystal Growth*, 2nd ed. (Elsevier B. V., Amsterdam, 2015), Vol. II.
[58]D. Ma, Front. Mech. Eng. **13**, 3 (2018).
[59]S. Zaefferer, J. C. Kuo, Z. Zhao, M. Winning, and D. Raabe, Acta Mater. **51**, 4719 (2003).
[60]X. Huang, A. Borrego, and W. Pantleon, Mater. Sci. Eng.: A **319**, 237 (2001).
[61]B. B. Blizanac, P. N. Ross, and N. M. Markovic, J. Phys. Chem. B **110**, 4735 (2006).
[62]P. J. Berlowitz, C. H. F. Peden, and D. W. Goodman, J. Phys. Chem. **92**, 5213 (1988).
[63]A. M. Gomez-Marin, R. Rizo, and J. M. Feliu, Catal. Sci. Technol. **4**, 1685 (2014).
[64]G. A. Somorjai, Acc. Chem. Res. **9**, 248 (1976).
[65]C. Hahn, T. Hatsukade, Y. G. Kim, A. Vailionis, J. H. Baricuatro, D. C. Higgins, S. A. Nitopi, M. P. Soriaga, and T. F. Jaramillo, Proc. Natl. Acad. Sci. U. S. A. **114**, 5918–5923 (2017).
[66]D. W. Goodman, Surf. Sci. **299**, 837 (1994).
[67]G. A. Tritsaris, J. Greeley, J. Rossmeisl, and J. K. Norskov, Catal. Lett. **141**, 909 (2011).

[68]Y. Suchorski and G. Rupprechter, Catal. Lett. **148**, 2947 (2018).
[69]T. Kuech, *Handbook of Crystal Growth*, 2nd ed. (Elsevier B. V., Amsterdam, 2014), Vol. III.
[70]P. Y. Huang, C. S. Ruiz-Vargas, A. M. van der Zande, W. S. Whitney, M. P. Levendorf, J. W. Kevek, S. Garg, J. S. Alden, C. J. Hustedt, Y. Zhu, J. Park, P. L. McEuen, and D. A. Muller, Nature **469**, 389 (2011).
[71]Q. K. Yu, L. A. Jauregui, W. Wu, R. Colby, J. F. Tian, Z. H. Su, H. L. Cao, Z. H. Liu, D. Pandey, D. G. Wei, T. F. Chung, P. Peng, N. P. Guisinger, E. A. Stach, J. M. Bao, S. S. Pei, and Y. P. Chen, Nat. Mater. **10**, 443 (2011).
[72]X. Mi, V. Meunier, N. Koratkar, and Y. F. Shi, Phys. Rev. B **85**, 155436 (2012).
[73]C. M. Seah, S. P. Chai, and A. R. Mohamed, Carbon **70**, 1 (2014).
[74]B. W. Li, D. Luo, L. Zhu, X. Zhang, S. Jin, M. Huang, F. Ding, and R. S. Ruoff, Adv. Mater. **30**, 1706504 (2018).
[75]B. Wang, D. Luo, Z. C. Li, Y. Kwon, M. H. Wang, M. Goo, S. W. Jin, M. Huang, Y. T. Shen, H. F. Shi, F. Ding, and R. S. Ruoff, Adv. Mater. **30**, 1800888 (2018).
[76]D. Luo, M. Wang, Y. Li, C. Kim, K. M. Yu, Y. Kim, H. Han, M. Biswal, M. Huang, Y. Kwon, M. Goo, D. C. Camacho-Mojica, H. Shi, W. J. Yoo, M. S. Altman, H. J. Shin, and R. S. Ruoff, Adv. Mater. **31**, 1903615 (2019).
[77]R. J. Chang, X. C. Wang, S. S. Wang, Y. W. Sheng, B. Porter, H. Bhaskaran, and J. H. Warner, Chem. Mater. **29**, 6252 (2017).
[78]X. J. Song, J. F. Gao, Y. F. Nie, T. Gao, J. Y. Sun, D. L. Ma, Q. C. Li, Y. B. Chen, C. H. Jin, A. Bachmatiuk, M. H. Ruemmeli, F. Ding, Y. F. Zhang, and Z. F. Liu, Nano Res. **8**, 3164 (2015).
[79]M. Ajmal, S. Lee, Y. C. Cho, S. J. Kim, S. E. Park, C. R. Cho, and S. Y. Jeong, CrystEngComm **14**, 1463 (2012).
[80]A. Goyal, M. P. Paranthaman, and U. Schoop, MRS Bull. **29**, 552 (2004).
[81]M. W. Rupich, X. P. Li, C. Thieme, S. Sathyamurthy, S. Fleshler, D. Tucker, E. Thompson, J. Schreiber, J. Lynch, D. Buczek, K. DeMoranville, J. Inch, P. Cedrone, and J. Slack, Supercond. Sci. Technol. **23**, 014015 (2010).
[82]T. G. Holesinger, L. Civale, B. Maiorov, D. M. Feldmann, J. Y. Coulter, J. Miller, V. A. Maroni, Z. J. Chen, D. C. Larbalestier, R. Feenstra, X. P. Li, M. B. Huang, T. Kodenkandath, W. Zhang, M. W. Rupich, and A. P. Malozemoff, Adv. Mater. **20**, 391 (2008).
[83]G. L. Messing, S. Poterala, Y. F. Chang, T. Frueh, E. R. Kupp, B. H. Watson, R. L. Walton, M. J. Brova, A. K. Hofer, R. Bermejo, and R. J. Meyer, J. Mater. Res. **32**, 3219 (2017).
[84]A. Goyal, D. P. Norton, D. K. Christen, E. D. Specht, M. Paranthaman, D. M. Kroeger, J. D. Budai, Q. He, F. A. List, R. Feenstra, H. R. Kerchner, D. F. Lee, E. Hatfield, P. M. Martin, J. Mathis, and C. Park, Appl. Supercond. **4**, 403 (1996).
[85]Y. Ogawa *et al.*, J. Phys. Chem. Lett. **3**, 219 (2012).